

A Framework of $SO(3)$ -equivariant Non-linear Representation Learning and its Application to Electronic-Structure Hamiltonian Prediction

Shi Yin^{1*}, Xinyang Pan², Fengyan Wang¹, Feng Wu^{3,1}, *Fellow of IEEE*, Lixin He^{2,1*}

^{1*}Institute of Artificial Intelligence, Hefei Comprehensive National Science Center, Hefei, 230088, People's Republic of China.

²CAS Key Laboratory of Quantum Information, University of Science and Technology of China, Hefei, 230026, People's Republic of China.

³University of Science and Technology of China, Hefei, 230026, People's Republic of China.

*Corresponding author(s). E-mail(s): shiyin@iai.ustc.edu.cn; helx@ustc.edu.cn;

Abstract

We present both a theoretical and a methodological framework that addresses a critical challenge in applying deep learning to physical systems: the reconciliation of non-linear expressiveness with $SO(3)$ -equivariance in predictions of $SO(3)$ -equivariant quantities, such as the electronic-structure Hamiltonian. Inspired by covariant theory in physics, we address this problem by exploring the mathematical relationships between $SO(3)$ -invariant and $SO(3)$ -equivariant quantities and their representations. We first construct theoretical $SO(3)$ -invariant quantities derived from the $SO(3)$ -equivariant regression targets, and use these invariant quantities as supervisory labels to guide the learning of high-quality $SO(3)$ -invariant features. Given that $SO(3)$ -invariance is preserved under non-linear operations, the encoding process for invariant features can extensively utilize non-linear mappings, thereby fully capturing the non-linear patterns inherent in physical systems. Building on this foundation, we propose a gradient-based mechanism to induce $SO(3)$ -equivariant encodings of various degrees from the learned $SO(3)$ -invariant features. This mechanism can incorporate non-linear expressive capabilities into $SO(3)$ -equivariant representations, while theoretically preserving their equivariant properties as we prove. Our approach offers a promising general

solution to the critical dilemma between equivariance and non-linear expressiveness in deep learning methodologies. We apply our theory and method to the electronic-structure Hamiltonian prediction tasks, demonstrating state-of-the-art performance across six benchmark databases.

Keywords: Deep Learning Theory, Neural Networks, SO(3)-equivariance, Science for AI, AI for Science

1 Introduction

With the advantages in computational complexity and generalization capabilities, deep learning paradigm has vigorously driven advancements in physics research [1]. For example, in predicting electronic-structure Hamiltonians, traditional Density Functional Theory (DFT) methods [2, 3] suffer from computational complexities of $\mathcal{O}(N^3)$. In contrast, deep learning approaches have significantly reduced this complexity to $\mathcal{O}(N)$ [4–7], accelerating processes by thousands or even millions of times. This reduction in computational demand not only unlocks possibilities for analyzing extremely large atomic systems but also paves the way for efficient material simulation, discovery, and design that were previously unimaginable.

However, deep learning methods still face substantial challenges when processing physical systems. To align with fundamental physical laws, these methods must strictly adhere to symmetry principles. For example, physical quantities such as force fields and electronic-structure Hamiltonians must be equivariant under 3D rotational transformations, i.e., elements from the SO(3) group. Traditional deep learning methods [8, 9] typically approximated SO(3)-equivariance through rotational data augmentation. However, this approach does not provide the strict assurance of SO(3)-equivariance required for physical research. Besides, the calculation of physical quantities calls for ultra-high numerical accuracy. For example, it is typically required that the errors on Hamiltonian calculation being restricted within the sub-millielectron volts (sub-meV) scale, to ensure accurate derivation of downstream physical quantities and related material properties. This necessitates that the neural networks possess strong capabilities to express the complex non-linear mappings from atomic structures to the regression targets. However, existing deep learning methods are unable to simultaneously ensure strict SO(3)-equivariance and high numerical accuracy. The root cause of this problem lies in the conflict between SO(3)-equivariance and non-linear expressiveness: specifically, directly applying non-linear activation functions on SO(3)-equivariant features (with degree $l \geq 1$) leads to the loss of equivariance, while bypassing non-linear mappings severely restricts the network’s expressive capabilities and thereby lowering down the achievable accuracy. Although several efforts have been made to address this challenge—introducing gated activation mechanisms [7, 10–12], developing local-coordinate approaches [6], and employing discrete spherical harmonic bases [13–15]—they still fall short, to varying degrees, of fully reconciling strict adherence to SO(3)-equivariance with the requirements for high-precision generalization capability. As analyzed in previous literature [13], this issue is commonly

found in machine learning tasks that demand both strict equivariance and fine-grained generalization performance.

To address this challenge, we make theoretical and methodological explorations on unifying strict $SO(3)$ -equivariance with strong non-linear expressiveness within the realm of deep representation learning. We are inspired by the insight that invariant quantities in transformation often reflect the mathematical nature of physical laws and can induce other quantities with equivariant properties. For example, in special relativity [17], the spacetime interval between events is an invariant under Lorentz transformations. This invariance is foundational in formulating physical laws that involve covariant quantities. Furthermore, from the perspective of deep representation learning, the attribute of preserving invariance under non-linear operations is a significant advantage, due to its compatibility with non-linear expressive capabilities. Built upon these insights, **we theoretically solve the equivariance-expressiveness dilemma by intensively exploring and making use of the intrinsic relationships between $SO(3)$ -invariant and $SO(3)$ -equivariant quantities and representations**: we first dedicate efforts to learning high-quality $SO(3)$ -invariant features with ample non-linear expressiveness, and subsequently, we derive $SO(3)$ -equivariant non-linear representations from these $SO(3)$ -invariant ones. Specifically:

First, we construct quantities that are theoretically $SO(3)$ -invariant, namely $tr(\mathbf{Q} \cdot \mathbf{Q}^\dagger)$, where \mathbf{Q} are the $SO(3)$ -equivariant regression targets, $tr(\cdot)$ signifies the trace operation, and \dagger denotes the conjugate transpose operation. A significant advantage of these $SO(3)$ -invariant quantities lies in the fact that they are directly derived from the $SO(3)$ -equivariant target labels and can serve as unique supervision labels for the effective learning of informative $SO(3)$ -invariant features that capture the intrinsic symmetry properties of the mathematical structure of \mathbf{Q} without requiring additional labeling resources.

Second, we propose a gradient-based mechanism to induce $SO(3)$ -equivariant representations as well as the regression target \mathbf{Q} , from high-quality $SO(3)$ -invariant features learned under the supervision of $tr(\mathbf{Q} \cdot \mathbf{Q}^\dagger)$. This mechanism can incorporate non-linear expressive capabilities into $SO(3)$ -equivariant representations while preserving their equivariant properties, as we prove.

We develop our theory into a unified $SO(3)$ -equivariant non-linear representation learning method, and apply it to the computation of electronic structure Hamiltonians, which are central to quantum physics and inherently complex, presenting substantial challenges for regression models. Our method significantly enhances the state-of-the-art performance on six benchmark Hamiltonian databases, demonstrating that our approach not only maintains strict $SO(3)$ -equivariance but also unleashes powerful non-linear expressiveness, thereby boosting the prediction accuracy of Hamiltonians, providing an effective deep learning tool for efficient and accurate electronic structure calculations of materials.

Our theory and method for bridging symmetry and expressiveness of deep learning are general and can be easily applied on predicting other physical quantities such as forces, which also obey $SO(3)$ -equivariance. Furthermore, it can also be extended to other application areas beyond physics. For instance, in some computer vision tasks, such as autonomous driving [18], where there is a high demand for robustness against

coordinate transformations of cameras, the mainstream approach has been to achieve approximate $SO(3)$ -equivariance through data augmentation. However, this does not guarantee absolute safety. Our work holds great potential to construct deep models with high generalization performance under the premise of strict $SO(3)$ -equivariance, potentially revolutionizing techniques in such tasks.

2 The Equivariance-Expressiveness Dilemma in Existing Deep Learning Methods

In this section, we introduce existing efforts to harmonize the deep learning paradigm with $SO(3)$ -equivariance, analyzing the dilemma between strict $SO(3)$ -equivariance and non-linear expressive capabilities.

2.1 Approaches with Strict $SO(3)$ -equivariance but Weak Expressiveness

Most existing methods have focused on achieving $SO(3)$ -equivariance at the neural mechanism level by applying group theory-guaranteed $SO(3)$ -equivariant operators [19, 20]. These operators, including linear scaling, element-wise sum, direct products, direct sums, and Clebsch-Gordan decomposition, have been used to build graph neural network architectures for tasks in 3D point cloud analysis [21], molecular dynamic simulation and property prediction [10, 11], as well as Hamiltonian prediction [4, 7, 12, 22]. However, these operators could not provide sufficient expressiveness to fit complex non-linear mappings. The majority of these operators are linear operations, and the only one (direct product) that introduces some non-linearity can only approximate a simple squaring function, and cannot be extended to more complex non-linear forms due to the huge computational burden and difficulty in convergence. Even worse, directly applying highly-expressive non-linear activation functions, such as *Sigmoid*, *Softmax*, and *SiLU*, to $SO(3)$ -equivariant features may result in the loss of equivariance. This dilemma leads to an unsatisfactory trade-off between strict equivariance and non-linear expressiveness, ultimately reducing the achievable performance of these regression models. To alleviate this issue, these methods introduced a gated activation mechanism that processes $SO(3)$ -invariant features ($l = 0$) using non-linear activations and employs them as linear gating coefficients for $SO(3)$ -equivariant features ($l \geq 1$), aiming to enhance their expressive power while maintaining strict equivariance. However, from the perspective of $SO(3)$ -equivariant features, this mechanism is a combination of linear operations and cannot fundamentally increase their non-linear expressive capabilities.

2.2 Approaches with Remarkable Expressiveness but Approximate $SO(3)$ -equivariance

Li et al. [6] proposed a local coordinate strategy to achieve $SO(3)$ -equivariance. This strategy relied on the transformation relationship between local and global coordinates to achieve equivariance, without imposing restrictions on the neural network, allowing the use of network modules that possess non-linear expressiveness. However, this

strategy, solely depending on coordinate transformations, only works under holistic rigid rotations of the atomic system. Without exploration of a neural mechanism for equivariance, when the local coordinates experience non-rigid perturbations such as thermal movements or bilayer twists, this strategy offers no guarantees on maintaining symmetry properties; Zitnick et al. [13] decomposed features into weighted sums of spherical harmonic basis functions, each corresponding to a discrete point on a unit sphere. Such discrete decomposition enables non-linear operations on the coefficients to enhance expressiveness. In subsequent developments [14, 15, 23], this approach has demonstrated a remarkable capacity to fit complex functions. However, it degenerates from continuous to discrete rotational equivariance, no longer maintaining strict equivariance to continuous rotational operations. In summary, although these methods with approximate SO(3)-equivariance achieve high numerical accuracy due to their extensive use of non-linear mechanisms, they are best suited for the applications that primarily require numerical approximations but not for tasks that demand theoretical depth in physics. In some applications, the demands for symmetry are extremely high. Even minor deviations from perfect symmetry can result in incorrect physical results.

Combining the analysis in this section, existing deep learning methods have compromised either strict SO(3)-equivariance or non-linear expressiveness when processing physical systems. In this paper, we develop a novel framework that theoretically combines strict SO(3)-equivariance with the non-linear expressiveness of neural networks. This solution resolves the equivariance-expressiveness dilemma by deeply exploring the intrinsic relationships between SO(3)-invariant and SO(3)-equivariant quantities.

3 Problem Formalization

Physical quantities that are SO(3)-equivariant typically possess their respective equivariant formulas under both matrix-formed direct-product states and vector-formed direct-sum states, which are mathematically equivalent to each other.

Without loss of generality, let $\mathbf{Q}^{l_p \otimes l_q}$ denote an SO(3)-equivariant quantity in direct-product state formed by $l_p \otimes l_q$, i.e., the direct product between degrees l_p and l_q . It obeys the following SO(3)-equivariant law:

$$\mathbf{Q}(\mathbf{R})^{l_p \otimes l_q} = \mathbf{D}^{l_p}(\mathbf{R}) \cdot \mathbf{Q}^{l_p \otimes l_q} \cdot (\mathbf{D}^{l_q}(\mathbf{R}))^\dagger, \quad 1 \leq p \leq P, 1 \leq q \leq Q \quad (1)$$

where \dagger denotes the conjugate transpose operation. $\mathbf{R} \in \mathbb{R}^{3 \times 3}$ is the rotational matrix and $\mathbf{D}^{l_p}(\mathbf{R}) \in \mathbb{R}^{(2l_p+1) \times (2l_p+1)}$, $\mathbf{D}^{l_q}(\mathbf{R}) \in \mathbb{R}^{(2l_q+1) \times (2l_q+1)}$ are the Wigner-D matrices of degrees l_p and l_q , respectively, $\mathbf{Q}(\mathbf{R})^{l_p \otimes l_q} \in \mathbb{R}^{(2l_p+1) \times (2l_q+1)}$ denotes the transformed results of $\mathbf{Q}^{l_p \otimes l_q} \in \mathbb{R}^{(2l_p+1) \times (2l_q+1)}$ through the rotational operation by \mathbf{R} .

$\mathbf{Q}^{l_p \otimes l_q}$ in the direct-product state can be further decomposed into a series of direct-sum state components with vector forms, i.e., $\mathbf{q}^l (|l_p - l_q| \leq l \leq l_p + l_q)$, which follows SO(3)-equivariant law mathematically equivalent to Eq. (1) but with a simpler form:

$$\mathbf{q}(\mathbf{R})^l = \mathbf{D}^l(\mathbf{R}) \cdot \mathbf{q}^l, \quad |l_p - l_q| \leq l \leq l_p + l_q \quad (2)$$

where $\mathbf{q}^l \in \mathbb{R}^{2l+1}$ and $\mathbf{q}(\mathbf{R})^l \in \mathbb{R}^{2l+1}$ respective denote the components with degree l before and after the rotational operation by \mathbf{R} .

Eq. (1) and Eq. (2) are mathematical equivalent to each other, meaning that fulfilling one under the corresponding state naturally satisfies the other. Due to the simplicity and ease of handling of the direct-sum state form, existing deep learning methods [6, 7] typically first predict $\mathbf{q}^l (|l_p - l_q| \leq l \leq l_p + l_q)$, then convert it to $\mathbf{Q}^{l_p \otimes l_q}$ through Clebsch-Gordan matrices. In the direct-sum state, to obey the equivariant law of Eq. (2) for the regression target, the hidden representations of neural networks must also satisfy the same form of equivariance:

$$\mathbf{f}(\mathbf{R})^{(k)l} = \mathbf{D}^l(\mathbf{R}) \cdot \mathbf{f}^{(k)l} \quad (3)$$

where $\mathbf{f}^{(k)l} \in \mathbb{R}^{2l+1}$ and $\mathbf{f}(\mathbf{R})^{(k)l} \in \mathbb{R}^{2l+1}$ respectively denote one channel of features with degree l before and after the rotational operation by \mathbf{R} , at the k th hidden layer.

Due to the intrinsic complexity and non-linearity of physic quantities, neural networks on regressing these quantities are supposed to equip with non-linear mappings denoted as $g_{nonlin}(\cdot)$ to fully capture the intrinsic patterns of the physical quantities, which is crucial for precise and generalizable prediction performance. Meanwhile, $g_{nonlin}(\cdot)$ must also preserve SO(3)-equivariance, which is expressed as:

$$\mathbf{f}(\mathbf{R})^{(k+1)l} = \mathbf{D}^l(\mathbf{R}) \cdot \mathbf{f}^{(k+1)l}, \mathbf{f}^{(k+1)l} = g_{nonlin}(\mathbf{f}^{(k)l}) \quad (4)$$

However, directly implementing $g_{nonlin}(\cdot)$ as neural network module with non-linear mechanisms, such as *Sigmoid*, *Softmax* and *Silu*, may result in the destruction of strict equivariance. How to make $g_{nonlin}(\cdot)$ both theoretically SO(3)-equivariant and capable of non-linear expressiveness, is the core problem this paper aims at solving.

4 Theory

This section establishes a rigorous theoretical foundation for integrating SO(3)-equivariance with non-linear expressiveness in the deep learning paradigm. First, we propose a theoretical construct to derive SO(3)-invariant quantities from the SO(3)-equivariant targets, aiming at facilitating the learning of high-quality SO(3)-invariant features. Second, we propose a gradient-based mechanism encoding features maintaining theoretically SO(3)-equivariance while possessing the non-linear expressive capability induced from SO(3)-invariant features to capture the complex non-linear patterns inherent in physical quantities.

Theorem 1. *The quantity $\mathbf{T} = tr(\mathbf{Q} \cdot \mathbf{Q}^\dagger)$ is SO(3)-invariant, where \mathbf{Q} is the simplified representation (without superscripts) of $\mathbf{Q}^{l_p \otimes l_q}$ defined in Section 3, and \dagger denotes the conjugate transpose operation, $tr(\cdot)$ is the trace operation.*

Proof. Under an SO(3) rotation represented by the rotational matrix \mathbf{R} , $\mathbf{Q} = \mathbf{Q}^{l_p \otimes l_q}$ is transformed as $\mathbf{Q}(\mathbf{R})$:

$$\mathbf{Q}(\mathbf{R}) = \mathbf{D}^{l_p}(\mathbf{R}) \cdot \mathbf{Q} \cdot \mathbf{D}^{l_q}(\mathbf{R})^\dagger,$$

where $\mathbf{D}^{l_p}(\mathbf{R})$ and $\mathbf{D}^{l_q}(\mathbf{R})$ are the Wigner-D matrices for the respective orbital degrees of atoms i and j , corresponding to the rotation \mathbf{R} .

The conjugate transpose of the transformed quantity is:

$$\mathbf{Q}(\mathbf{R})^\dagger = \mathbf{D}^{l_q}(\mathbf{R}) \cdot \mathbf{Q}^\dagger \cdot \mathbf{D}^{l_p}(\mathbf{R})^\dagger.$$

Thus, the product $\mathbf{Q}(\mathbf{R}) \cdot \mathbf{Q}(\mathbf{R})^\dagger$ is:

$$\mathbf{Q}(\mathbf{R}) \cdot \mathbf{Q}(\mathbf{R})^\dagger = (\mathbf{D}^{l_p}(\mathbf{R}) \cdot \mathbf{Q} \cdot \mathbf{D}^{l_q}(\mathbf{R})^\dagger) \cdot (\mathbf{D}^{l_q}(\mathbf{R}) \cdot \mathbf{Q}^\dagger \cdot \mathbf{D}^{l_p}(\mathbf{R})^\dagger).$$

Using the cyclic property of the trace, which states that the trace of a product of matrices remains unchanged under cyclic permutations (i.e., $tr(ABC) = tr(BCA) = tr(CAB)$), and combining the properties that $\mathbf{D}^{l_p}(\mathbf{R}) \cdot \mathbf{D}^{l_p}(\mathbf{R})^\dagger = \mathbf{I}$ and $\mathbf{D}^{l_q}(\mathbf{R}) \cdot \mathbf{D}^{l_q}(\mathbf{R})^\dagger = \mathbf{I}$, we can rearrange the terms inside the trace as follows:

$$\begin{aligned} \mathbf{T}(\mathbf{R}) &= tr(\mathbf{Q}(\mathbf{R}) \cdot \mathbf{Q}(\mathbf{R})^\dagger) = tr((\mathbf{D}^{l_p}(\mathbf{R}) \cdot \mathbf{Q} \cdot \mathbf{D}^{l_q}(\mathbf{R})^\dagger) \cdot (\mathbf{D}^{l_q}(\mathbf{R}) \cdot \mathbf{Q}^\dagger \cdot \mathbf{D}^{l_p}(\mathbf{R})^\dagger)) \\ &= tr(\mathbf{D}^{l_p}(\mathbf{R}) \cdot \mathbf{Q} \cdot \mathbf{Q}^\dagger \cdot \mathbf{D}^{l_p}(\mathbf{R})^\dagger) = tr(\mathbf{Q} \cdot \mathbf{Q}^\dagger \cdot \mathbf{D}^{l_p}(\mathbf{R})^\dagger \cdot \mathbf{D}^{l_p}(\mathbf{R})) = tr(\mathbf{Q} \cdot \mathbf{Q}^\dagger) = \mathbf{T}. \end{aligned}$$

Therefore, $\mathbf{T} = tr(\mathbf{Q} \cdot \mathbf{Q}^\dagger)$ is invariant under $SO(3)$ transformations, its $SO(3)$ -invariance is proved. \square

Theorem 2. *The non-linear neural mapping defined as the following is $SO(3)$ -equivariant:*

$$\mathbf{v} = g_{nonlin}(\mathbf{f}) = \frac{\partial(s_{nonlin}(CGDecomp(\mathbf{f} \otimes \mathbf{f}, 0)))}{\partial \mathbf{f}} \quad (5)$$

where \mathbf{f} is an input $SO(3)$ -equivariant feature with degree l in the direct-sum state, \otimes denotes the direct product operation, $CGDecomp(\cdot, 0)$ refers to performing a Clebsch-Gordan decomposition of the tensor and returning the scalar component of degree 0, and $s_{nonlin}(\cdot)$ represents non-linear neural mappings, \mathbf{v} is the features encoded by $g_{nonlin}(\cdot)$

Proof. The input feature \mathbf{f} is $SO(3)$ -equivariant, meaning that under an $SO(3)$ rotation represented by \mathbf{R} , it transforms as follows:

$$\mathbf{f}(\mathbf{R}) = \mathbf{D}^l(\mathbf{R}) \cdot \mathbf{f}$$

where $\mathbf{D}^l(\mathbf{R})$ is the Wigner-D matrix corresponding to degree l .

First, according to group theory, $u = CGDecomp(\mathbf{f} \otimes \mathbf{f}, 0)$ is an $SO(3)$ -invariant scalar because the degree-zero component from the Clebsch-Gordan decomposition is invariant under rotations. Since applying a non-linear operation to a $SO(3)$ -invariant quantity does not change its invariance, $z = s_{nonlin}(u)$ is also $SO(3)$ -invariant, independent to the specific form of $s_{nonlin}(\cdot)$. It formally holds that:

$$z = z(\mathbf{R}) \quad (6)$$

Next, we apply the chain rule in Jacobian form. Considering $\mathbf{f}(\mathbf{R})$ is a column vector, to facilitate the application of the chain rule in vector form, we first transpose it into

a row vector $\mathbf{f}(\mathbf{R})^T$, then differentiate:

$$\frac{\partial z(\mathbf{R})}{\partial \mathbf{f}^T(\mathbf{R})} = \frac{\partial z}{\partial \mathbf{f}^T(\mathbf{R})} = \frac{\partial z}{\partial \mathbf{f}^T} \frac{\partial \mathbf{f}^T}{\partial \mathbf{f}(\mathbf{R})^T} = \frac{\partial z}{\partial \mathbf{f}^T} \cdot \mathbf{D}^l(\mathbf{R})^{-1} = \frac{\partial z}{\partial \mathbf{f}^T} \cdot \mathbf{D}^l(\mathbf{R})^T \quad (7)$$

Here we utilize the property that $\mathbf{D}^l(\mathbf{R})^{-1} = \mathbf{D}^l(\mathbf{R})^T$. Since the representations of neural networks are generally real numbers, the Wigner-D matrix is also real unitary.

Finally, we transpose the result back to a column vector:

$$\mathbf{v}(\mathbf{R}) = g_{\text{nonlin}}(\mathbf{f}(\mathbf{R})) = \left(\frac{\partial z(\mathbf{R})}{\partial \mathbf{f}^T(\mathbf{R})} \right)^T = \left(\frac{\partial z}{\partial \mathbf{f}^T} \cdot \mathbf{D}^l(\mathbf{R})^T \right)^T = \mathbf{D}^l(\mathbf{R}) \cdot \frac{\partial z}{\partial \mathbf{f}} = \mathbf{D}^l(\mathbf{R}) \cdot \mathbf{v} \quad (8)$$

This proves that $g_{\text{nonlin}}(\cdot)$ is a $SO(3)$ -equivariant non-linear operator: when applying its non-linearity to a $SO(3)$ -equivariant feature \mathbf{f} , the output feature \mathbf{v} remains $SO(3)$ -equivariant. \square

Remark 1. In Theorem 1, the term $\text{tr}(\mathbf{Q} \cdot \mathbf{Q}^\dagger)$ is equal to the square of the Frobenius norm of the matrix \mathbf{Q} , i.e., $\text{tr}(\mathbf{Q} \cdot \mathbf{Q}^\dagger) = \|\mathbf{Q}\|_F^2 = \sum_{m,n} |\mathbf{Q}_{mn}|^2$. The invariance of Frobenius norm under unitary transformations reflects the profound connections between modulus and invariance in physics.

Remark 2. In Theorem 2, $g_{\text{nonlin}}(\cdot)$ can handle equivariant features of any degree and the returned feature \mathbf{v} has the same degree l as the input feature \mathbf{f} . \mathbf{v} is endowed with non-linear expressiveness with the effect of $s_{\text{nonlin}}(\cdot)$, which can be any differentiable non-linear network module, including non-linear activation functions and normalization operations. The gradient operation $\frac{\partial z}{\partial \mathbf{f}}$ in $g_{\text{nonlin}}(\cdot)$ is used during the forward inference process to promote feature encoding, expanding the usage and significance of gradients within the neural network paradigm. It is worth noting that, although the internal representations of neural network modules including $g_{\text{nonlin}}(\cdot)$ are in the real field, they are still able to predict targets in complex field with equivariance. Literature [7] has provided mechanisms for converting the network outputs in the real field into regression targets with real and imaginary parts.

Remark 3. z in Equation (6) is the bridge connecting Theorem 1 and Theorem 2 in implementing a $SO(3)$ -equivariant non-linear representation learning approach. Since z is an $SO(3)$ -invariant feature, it can be learned by $s_{\text{nonlin}}(\cdot)$, i.e., the neural mechanisms with non-linear expressive capability, through supervised learning incorporated with the $SO(3)$ -invariant label $\text{tr}(\mathbf{Q} \cdot \mathbf{Q}^\dagger)$. Following this, by taking the gradient of z with respect to \mathbf{f} , the non-linear expressiveness of z is transferred to the equivariant feature \mathbf{v} , while maintaining strict $SO(3)$ -equivariance as proved above. Subsequently, merging \mathbf{v} and \mathbf{f} , and applying $g_{\text{nonlin}}(\cdot)$ in a stacked manner can yield rich $SO(3)$ -equivariant non-linear representations.

Based on the new theory, we present a general method for learning non-linear representations that are equivariant to $SO(3)$, as shown in Figure 1. The core of our method can be abstractly referred to as **TraceGrad**. At the label level, it incorporates an $SO(3)$ -invariant **trace** quantity introduced in Theorem 1 as a supervisory signal for learning $SO(3)$ -invariant features; at the representation level, it induces non-linear

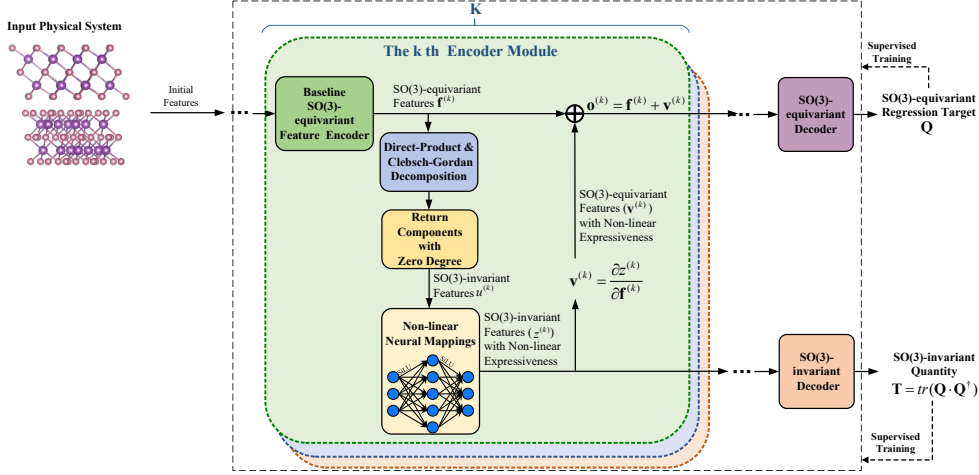


Fig. 1: Methodological framework for learning SO(3)-equivariant representations with non-linear expressiveness to regress complex SO(3)-equivariant targets.

SO(3)-equivariant features from non-linear SO(3)-invariant features through **gradient**-based operator introduced in Theorem 2. For details of the method, please refer to Section 8.

5 Application to the Hamiltonian Prediction Tasks

The tasks of predicting electronic-structure Hamiltonian are chosen as the application study of our theoretical and methodological framework, on two motivations. On one hand, the Hamiltonian occupies a central position in quantum mechanics. From the Hamiltonian, key physical quantities such as charge density, band structure, and Berry phase can be calculated, bringing deeply understanding of the electrical, optical, magnetic, and transport properties of atomic systems. On the other hand, the intrinsic symmetry with respect to the SO(3) group as well as the high-dimensional complexity (as shown in Figure 2) of the Hamiltonian provide a challenging touchstone of whether a deep learning method possesses both SO(3)-equivariance and strong expressive power.

Experiments are conducted on six benchmark databases of atomic systems that have Hamiltonian annotations, all of which are established and released by previous literature [6, 7]. These databases include:

- Monolayer Graphene (*MG*). This structure consists of a single layer of carbon atoms in a hexagonal lattice. It is known for its exceptional thermal conductivity, electrical properties, and mechanical strength. The potential applications of monolayer graphene extend across electronics, energy storage devices, and composite materials due to its unique properties. In the benchmark of *MG*, the sizes of the training set, validation set, and testing set are 270, 90, and 90 respectively.

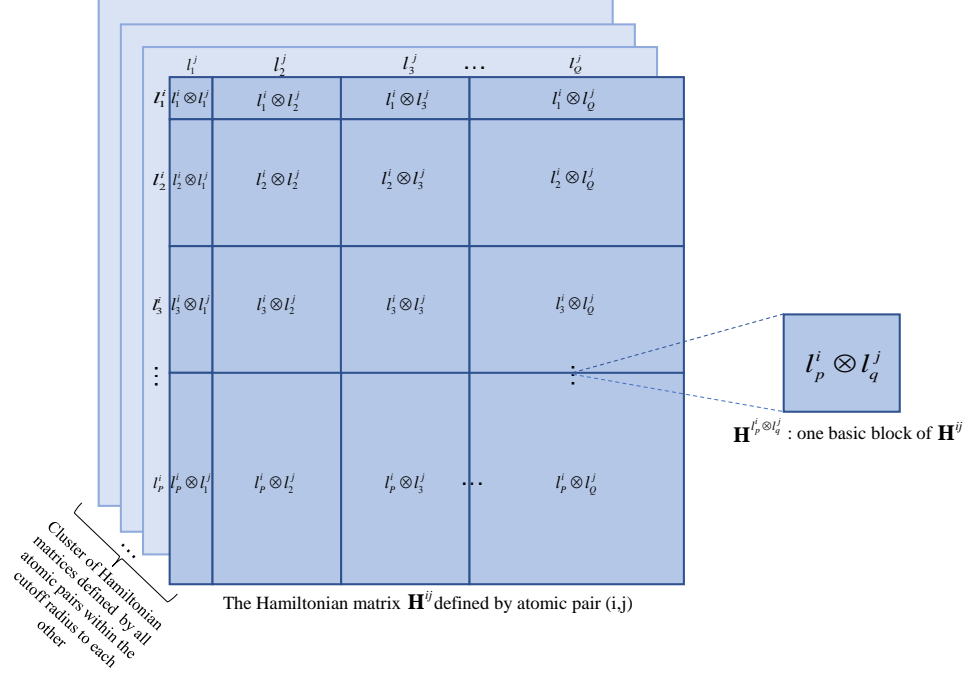


Fig. 2: Illustration of the high-dimensional complexity of the Hamiltonian. In an atomic system, a Hamiltonian matrix is defined between each pair of atoms within each other’s cutoff radius, constituting a large cluster of Hamiltonian matrices for all atom pairs. Besides, each Hamiltonian matrix contains multiple basic blocks, with the $\mathbf{Q}^{l_p \otimes l_q}$ defined in Section 3 corresponding to a basic block $\mathbf{H}^{l_p \otimes l_q}$ here. Thus, for a Hamiltonian prediction model, the space of the regression target is typically huge.

- Monolayer MoS2 (*MM*), which is a single layer of molybdenum disulfide and part of the transition metal dichalcogenides (TMDCs) group. This kind of structures is a semiconductor with a direct bandgap, making it suitable for optoelectronics, photovoltaics, and semiconducting components. It also shows promise in applications requiring high sensitivity to chemicals, making it valuable for sensors. In the benchmark of *MM*, the sizes of the training set, validation set, and testing set are 300, 100, and 100 respectively.

- Bilayer Graphene (*BG*), which consists of two layers of graphene stacked together. This kind of structures exhibits unique electronic properties such as tunable bandgap and enhanced conductivity when subjected to an electric field. Bilayer Graphene is being explored for use in advanced electronic devices, such as fast transistors and efficient batteries. In the benchmark database of *BG*, the sizes of the training set and validation set are 180 and 60 respectively, all of them are non-twisted samples; in the testing set, the numbers of non-twisted and twisted samples are 60 and 9 respectively.

- Bilayer Bismuthene (*BB*), which consists of two layers of bismuth atoms arranged in a honeycomb-like structure. This kind of materials shows potential for topological

insulating properties and has significant implications for quantum computing and spintronic devices due to its strong spin-orbit coupling. In the benchmark of *BB*, the sizes of the training set and validation set are 231 and 113 respectively, all of them are non-twisted samples; in the testing set, the numbers of non-twisted and twisted samples are 113 and 4 respectively.

- Bilayer Bi₂Te₃ (*BT*), which is a compound of bismuth and tellurium, known for its thermoelectric properties. This kind of structures is particularly valuable in thermoelectric devices for power generation and refrigeration technologies where waste heat can be converted into electrical energy. In the benchmark of *BT*, the sizes of the training set and validation set are 204 and 38 respectively, all of them are non-twisted samples; in the testing set, the numbers of non-twisted and twisted samples are 12 and 2 respectively.

- Bilayer Bi₂Se₃ (*BS*), another bismuth-tellurium compound, similar to Bi₂Te₃ but with selenium replacing tellurium. It also exhibits excellent thermoelectric properties and potential for topological insulator applications. This makes it suitable for energy harvesting applications and advanced electronic devices based on topological insulator technology. In the benchmark of *BS*, the sizes of the training set and validation set are 231 and 113 respectively, all of them are non-twisted samples; in the testing set, the numbers of non-twisted and twisted samples are 113 and 2 respectively.

These databases are both diverse and representative. They encompass both strong chemical bonds between single-layer atoms and weaker van der Waals interactions between bilayers, and also cover varying degrees of Spin-Orbit Coupling (SOC) effects: structures like *BT*, *BB*, and *BS* exhibit strong SOC effects, while others have weak SOC. These atomic structures are highly valuable in the field of information and energy science and technology. Yet, accurately predicting their Hamiltonians poses significant challenges due to structural deformations from thermal movements and inter-layer twists, as depicted in Fig. 3, where the twisted structures have garnered considerable attention as a research focus because of their potential to exhibit novel electrical properties and quantum topological behaviors [24, 25]. During twisting, the relative rotation between atoms and their coordinate system introduces SO(3)-equivariant effects, while changes in orientation between two layers alter the vdW interactions. These dynamic conditions challenge both the equivariance and expressive capabilities of the regression model. In our experiments, predicting the Hamiltonian of twisted samples are even challenging, as we strictly adhere to the official division of training, validation, and testing sets as defined upon the dataset’s release¹. In this division, twisted samples are only included in the testing set and are absent from the training set. This setup forces the regression model to solely rely on its generalization ability and the inherent SO(3)-equivariance to extrapolate the twisting conditions.

In summary, these benchmarks present scientific challenges for a regression model, pushing the boundaries of modeling capabilities in predicting complex quantum behaviors under dynamic conditions.

¹<https://github.com/Xiaoxun-Gong/DeepH-E3>

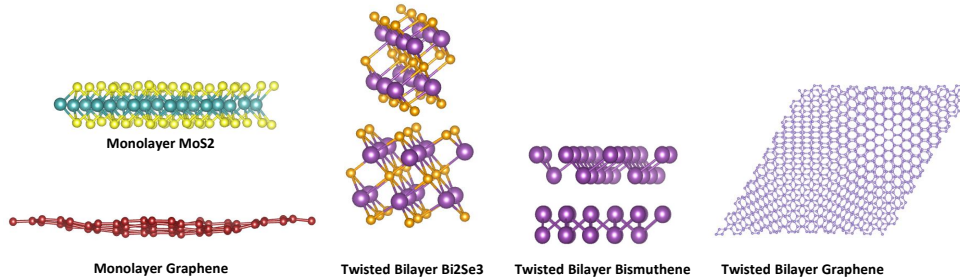


Fig. 3: Illustration of challenging samples in the experimental databases, showing structural distortions of atomic systems due to thermal movements and twists between the two layers, which require a regression model to possess both strict $\text{SO}(3)$ -equivariance and strong expressive capacity.

6 Results and Analysis

To validate the effectiveness of the proposed method, we compare results from the four setups:

- **Baseline model (DeepHE3 [7]):** We select DeepHE3 as our baseline model since it represents the state-of-the-art (SOTA) among strictly $\text{SO}(3)$ -equivariant approaches for predicting electronic-structure Hamiltonians. This choice facilitates further breakthroughs based on the SOTA foundation. DeepHE3 is trained using the mean squared error (MSE) loss of the Hamiltonian. In the subsequent experimental setups, DeepHE3 will serve as a base encoder, providing basic $\text{SO}(3)$ -equivariant features that are handled by our method as more expressive representations.

- **DeepHE3+Trace:** This experimental setup, an ablation term, only implements half part of our method. Specifically, it extends the architecture of DeepHE3 by adding our $\text{SO}(3)$ -invariant encoding and decoding branches and using the **trace** quantity $\mathbf{T} = \text{tr}(\mathbf{Q} \cdot \mathbf{Q}^\dagger) = \text{tr}(\mathbf{H}^{l_p \otimes l_q} \cdot (\mathbf{H}^{l_p \otimes l_q})^\dagger)$ to train them. As for ablation study, this setup does not include mechanisms for encoding non-linear $\text{SO}(3)$ -equivariant features via the gradient-induced operator; instead, it directly uses the features outputted by DeepHE3 for Hamiltonian regression.

- **DeepHE3+Grad:** This setup is also an ablation term and implements the other half part of our method in contrast to the previous ablation term. Specifically, it incorporates our $\text{SO}(3)$ -invariant encoder branch as well as the **gradient**-induced operator to yield $\text{SO}(3)$ -equivariant non-linear features based on the representations provided by the base encoders of DeepHE3 for Hamiltonian prediction. As for ablation study, this setup continues to use the single-task training pipeline of DeepHE3, predicting only the Hamiltonian without joint supervision training through the trace label.

- **DeepHE3+TraceGrad.** This setup corresponds to a complete implementation of our framework. Extending beyond the baseline architecture and pipeline of DeepHE3, at the label level, we introduce the **trace** quantity to guide the learning of $\text{SO}(3)$ -invariant features; Meanwhile, at the representation level, we leverage non-linear $\text{SO}(3)$ -invariant features induced by the **gradient** operator to yield non-linear $\text{SO}(3)$ -equivariant features for Hamiltonian prediction.

Table 1: Comparison on the MAE_{all} , MAE_{sample}^{cha} and MAE_{block}^{cha} metrics (/meV) for the four experimental setups on the databases of monolayer structures.

Methods	MG			MM		
	MAE_{all}	MAE_{sample}^{cha}	MAE_{block}^{cha}	MAE_{all}	MAE_{sample}^{cha}	MAE_{block}^{cha}
DeepHE3 (Baseline)	0.251	0.357	0.362	0.406	0.574	1.103
DeepHE3+Trace	0.230	0.344	0.348	0.378	0.537	1.091
DeepHE3+Grad	0.185	0.269	0.258	0.308	0.453	0.924
DeepHE3+TraceGrad	0.175	0.257	0.228	0.285	0.412	0.808

The performance of interest for the electronic-structure Hamiltonian prediction task are SO(3)-equivariance and numerical accuracy. Our method has already been theoretically proven to strictly obey SO(3)-equivariance in Section 4; therefore, we just focus on evaluating numerical accuracy here. Four metrics are adopted, i.e., MAE_{all} , which calculates the Mean Absolute Error (MAE) averaged across all elements of the Hamiltonian matrices from all testing samples in the current database; MAE_{sample}^{cha} , which calculates the MAE on the most challenging testing samples where the baseline model (DeepHE3) performs the worst in the current database; MAE_{block} , which calculates the MAE for each basic block of the Hamiltonian matrix, averaged across all testing samples in the current database; MAE_{block}^{cha} , which corresponds to the MAE on the most challenging Hamiltonian block where the baseline model shows the poorest performance (with the largest MAE_{block}) in the current dataset. These metrics comprehensively reflect the accuracy performance, considering not only the average accuracy but also the accuracy on difficult samples and challenging blocks of the Hamiltonian matrices.

We collect results from 10 independently repeated experiments on each database and list them in Tables 1 and 2, including the values of MAE_{all} , MAE_{sample}^{cha} , and MAE_{block}^{cha} , for monolayer and bilayer structures, respectively. Considering the large volume of statistics on MAE_{block} for all blocks, we just display the complete results in Figures 4 and 5 with the form of bar charts for DeepHE3 and DeepHE3+TraceGrad. As we use a fixed random seed (42) for all of the experiments, we find that the standard deviation of each metric is very small (all less than 0.007 meV) across the 10 repeated experiments. Since the fluctuation is negligible, in the following tables and figures, we just present the mean values of MAE_{all} , MAE_{sample}^{cha} , and MAE_{block}^{cha} across the repeated experiments, without listing the standard deviations of each entry to save space.

Table 2: Comparison on the MAE_{all} , MAE_{sample}^{cha} and MAE_{block}^{cha} metrics (/meV) for the four experimental setups on the databases of bilayer structures, where the superscripts nt and t respectively denote the non-twisted and twisted subsets.

Methods	BG^{nt}			BG^t		
	MAE_{all}	MAE_{sample}^{cha}	MAE_{block}^{cha}	MAE_{all}	MAE_{sample}^{cha}	MAE_{block}^{cha}
DeepHE3 (Baseline)	0.389	0.453	0.644	0.264	0.429	0.609
DeepHE3+Trace	0.362	0.417	0.593	0.251	0.401	0.480
DeepHE3+Grad	0.320	0.356	0.511	0.222	0.389	0.446
DeepHE3+TraceGrad	0.291	0.323	0.430	0.198	0.372	0.406
Methods	BB^{nt}			BB^t		
	MAE_{all}	MAE_{sample}^{cha}	MAE_{block}^{cha}	MAE_{all}	MAE_{sample}^{cha}	MAE_{block}^{cha}
DeepHE3 (Baseline)	0.274	0.304	1.042	0.468	0.602	2.399
DeepHE3+Trace	0.259	0.285	0.928	0.429	0.570	1.782
DeepHE3+Grad	0.243	0.272	0.824	0.406	0.542	1.431
DeepHE3+TraceGrad	0.226	0.256	0.740	0.384	0.503	1.284
Methods	BT^{nt}			BT^t		
	MAE_{all}	MAE_{sample}^{cha}	MAE_{block}^{cha}	MAE_{all}	MAE_{sample}^{cha}	MAE_{block}^{cha}
DeepHE3 (Baseline)	0.447	0.480	1.387	0.831	0.850	4.572
DeepHE3+Trace	0.406	0.462	1.239	0.784	0.812	4.520
DeepHE3+Grad	0.342	0.365	0.750	0.742	0.786	4.463
DeepHE3+TraceGrad	0.295	0.312	0.718	0.735	0.755	4.418
Methods	BS^{nt}			BS^t		
	MAE_{all}	MAE_{sample}^{cha}	MAE_{block}^{cha}	MAE_{all}	MAE_{sample}^{cha}	MAE_{block}^{cha}
DeepHE3 (Baseline)	0.397	0.424	0.867	0.370	0.390	0.875
DeepHE3+Trace	0.382	0.397	0.843	0.351	0.367	0.838
DeepHE3+Grad	0.343	0.365	0.696	0.324	0.339	0.746
DeepHE3+TraceGrad	0.300	0.332	0.644	0.291	0.302	0.674

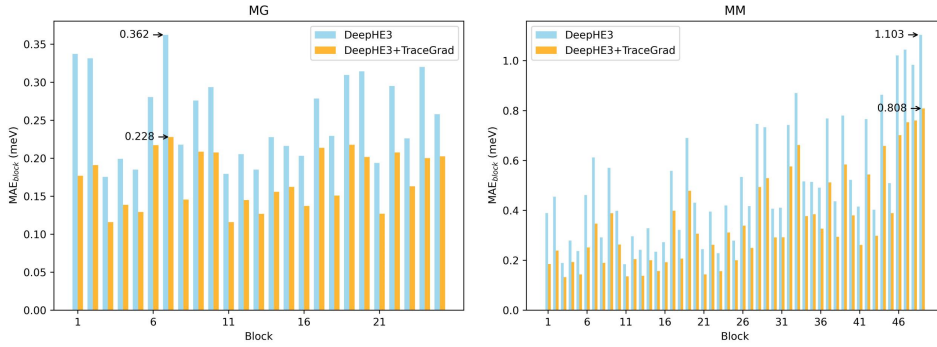


Fig. 4: MAE_{block} on each basic block of the Hamiltonian matrices of monolayer structures.

Combining the results from Table 1, Table 2, Figure 4 and Figure 5, we find that the proposed TraceGrad method significantly enhances the accuracy performance of the baseline method DeepHE3, both on average and for challenging samples or blocks, both on the non-twisted samples and the twisted samples marking strong difficulty for the expressive power and generalization ability of regression models as analyzed in Section 5. Specifically, TraceGrad lowers down the MAE_{all} of DeepHE3 with a relative ratio of 30.28%, 29.80%, 25.19%, 25.00%, 17.52%, 17.95%, 34.00%, 11.55%, 24.43%, and 21.35%, on MG , MM , BG^{nt} , BG^t , BB^{nt} , BB^t , BT^{nt} , BT^t , BS^{nt} , and BS^t , respectively; and lowering down MAE_{cha} by 28.01%, 28.22%, 28.70%, 13.29%, 15.79%, 16.45%, 35.00%, 11.18%, 21.70%, and 22.56%, on the respective datasets; and achieving better results in the vast majority of basic blocks. Particularly, for the blocks where DeepHE3 performs the worst, TraceGrad reduces the MAE (MAE_{block}^{cha}) by 37.01%, 26.75%, 33.23%, 33.33%, 28.98%, 46.48%, 48.23%, 3.37%, 25.72%, and 22.97%, on the respective datasets, from which the MAE_{block}^{cha} in MM , BG^{nt} and BT^{nt} are lowered down to within $1meV$; the MAE_{block}^{cha} in BB^t is decreased by nearly half to approach $1meV$. This indicates that the proposed representation learning framework, while maintaining strict $SO(3)$ -equivariance, significantly enhances the expressiveness of equivariant representations, thereby showcasing immense advantages in capturing the complexity of physical systems and refreshing the SOTA accuracy on the six benchmark databases.

From the results of ablation terms, we can obtain a more fine-grained experimental analysis. By comparing among the results of DeepHE3, DeepHE3+Trace, DeepHE3+Grad, and DeepHE3+TraceGrad, we can conclude that the two core mechanisms of our method, i.e., the $SO(3)$ -invariant trace supervision mechanism (Trace) at the label level as well as the gradient-based induction mechanism (Grad) at the representation layer, can contribute to the performance individually. Moreover, their combination provides even better performance. This is because, on one hand, with the gradient-based induction mechanism as a bridge, the $SO(3)$ -invariant features learned from the trace label can be transformed into the $SO(3)$ -equivariant representations during inference; on the other hand, with trace label, the $SO(3)$ -invariant network branch has a strong supervisory signal, enabling it to learn the intrinsic symmetry and complexity of the regression targets, which enhances the quality of $SO(3)$ -invariant features and ultimately benefits the encoding of $SO(3)$ -equivariant features. The value of such complementarity has been fully demonstrated in the experimental results.

7 Future Work

In future research, various extensions are conceivable across theoretical, methodological, and application fields. Theoretically, we can generalize $SO(3)$ group symmetry to a broader range and more complex groups. This will enable deep learning frameworks to accommodate richer mathematical structures. From a methodological perspective, this study employs the DeepHE3 framework for comparative purposes. However, it is feasible to adopt a more sophisticated network, such as the Transformer-based $SO(3)$ -equivariant non-linear representation learning framework, which utilizes the general

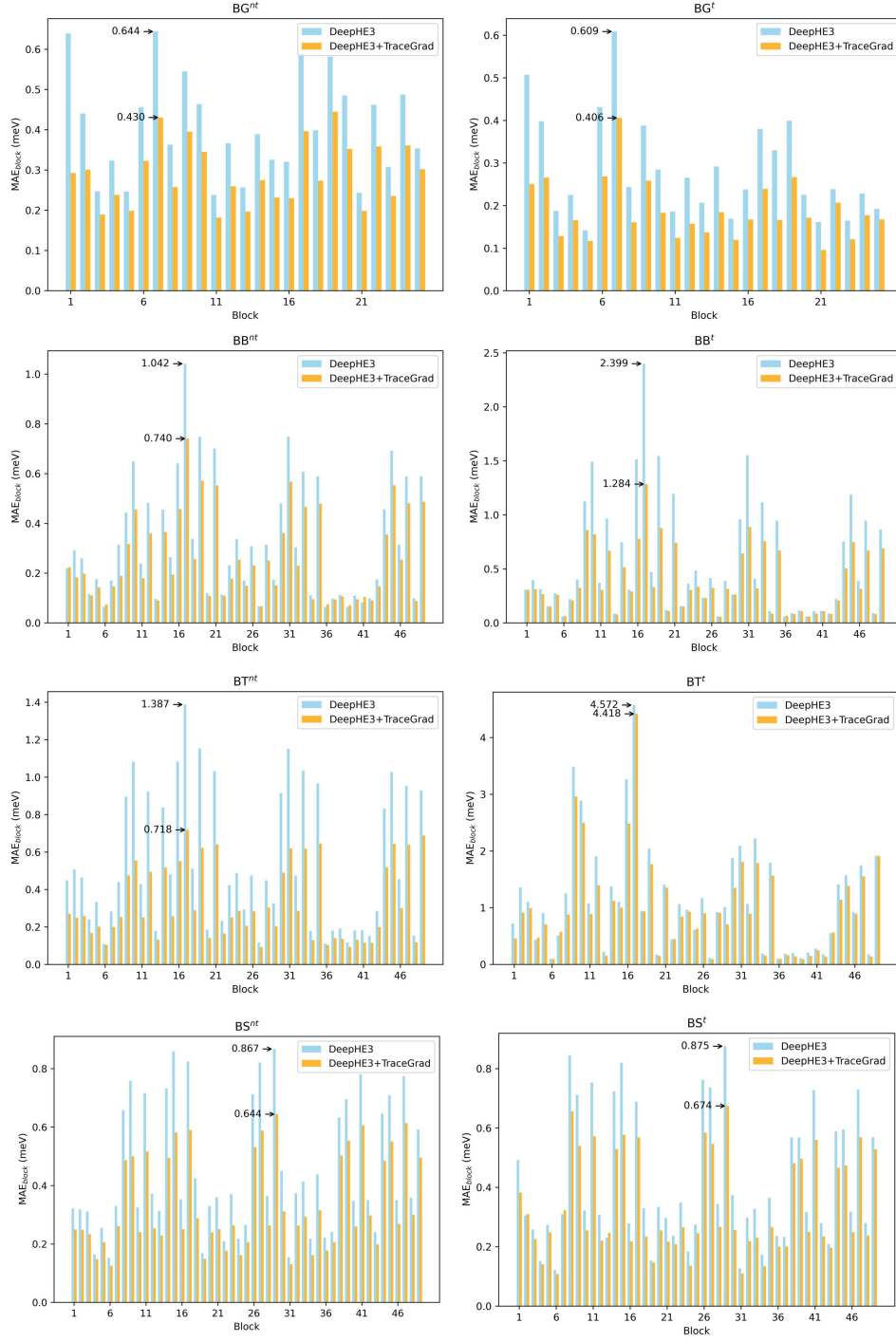


Fig. 5: MAE_{block} on each basic block of the Hamiltonian matrix in non-twisted (marked by superscripts nt) and twisted (marked by superscripts t) bilayer structures.

TraceGrad methodology. The current methodology extends beyond predicting electronic Hamiltonians and is capable of generally predicting multiple physical quantities and properties that require equivariance. Furthermore, the methodology is not confined to physical research alone and may find applications in areas such as robotics, autonomous vehicles, and motion tracking systems. It handles 3D point cloud data and other vision information to achieve safer and more reliable prediction results with SO(3)-symmetry. Looking forward to future endeavors, the foundational and pivotal role of this work is clear.

8 Method

8.1 Encoding and Decoding Framework

As shown in Figure 1, our encoding framework corresponds to a total of K encoding modules, which are sequentially connected to form a cascading stack. For the k -th module ($1 \leq k \leq K$), it first introduces an SO(3)-equivariant base encoder, e.g., the encoder from DeepHE3 [7] which is composed of recently developed equivariant operators [19, 20] like linear scaling, direct products, direct sums, Clebsch-Gordan decomposition, gated activation, equivariant normalization, and etc., to encode the physical system’s initial representations, such as spherical harmonics [26], or representations passed from the previous neural layers, as equivariant features $\mathbf{f}^{(k)}$ in the current hidden layer. Next, we construct the feature $\mathbf{v}^{(k)} = g_{\text{nonlin}}(\mathbf{f}^{(k)})$, to achieve sufficient non-linear expressiveness while maintaining SO(3)-equivariance, where $g_{\text{nonlin}}(\cdot)$ is the function defined in Equation (5). As for $s_{\text{nonlin}}(\cdot)$, i.e., the built-in non-linear mechanism within $g_{\text{nonlin}}(\cdot)$, although it can be implemented as any differentiable non-linear neural module, here for simplicity, we implement it as a fully connected feed-forward structure containing the SiLU activation function and layer normalization. To facilitate learning and optimization, we connect the input and output of $g_{\text{nonlin}}(\cdot)$ in a residual manner [27], serving as the output of the current encoding module, i.e., $\mathbf{o}^{(k)} = \mathbf{f}^{(k)} + \mathbf{v}^{(k)}$. $\mathbf{o}^{(k)}$ is then fed into the next encoder module to yield $\mathbf{f}^{(k+1)}$, $\mathbf{o}^{(k+1)}$, ..., until the last encoder module, which is followed by the decoder modules.

For an expressive feature encoder handling a complex physical system, $\mathbf{f}^{(k)}$ is usually not a feature of single degree but a direct-sum concatenation of series of components $\mathbf{f}^{(k)l_1}$, $\mathbf{f}^{(k)l_2}$, ..., $\mathbf{f}^{(k)l_k}$ at multiple degrees, i.e., l_1 , l_2 , ..., l_k , where some components share the same degree while others differ. In this case, it becomes necessary to extend the decomposition operator, i.e., CGDecomp(\cdot) in Equation (5), to accommodate various components of degrees. Moreover, in the context of neural networks, introducing learnable parameters W may improve the model capacity. Based on these considerations, when constructing the encoding module, the CGDecomp(\cdot) operation in Equation (5) can be expanded as CGDecomp_{ext}(\cdot):

$$u^{(k)} = \text{CGDecomp}_{\text{ext}}(\mathbf{f}^{(k)} \otimes \mathbf{f}^{(k)}, 0, W) = \sum_{1 \leq i, j \leq k, l_i = l_j} W_{ij} \cdot \text{CGDecomp}(\mathbf{f}^{(k)l_i} \otimes \mathbf{f}^{(k)l_j}, 0) \quad (9)$$

where W represents learnable parameters. This expansion does not change the equivariance or invariance of the features. It is obvious that, the output ($u^{(k)}$) of

$\text{CGDecomp}_{\text{ext}}(\cdot)$ is also $\text{SO}(3)$ -invariant, just like the original $\text{CGDecomp}(\cdot)$. Thus, even with such an expansion, the features $z^{(k)} = s_{\text{nonlin}}(u^{(k)})$ remain $\text{SO}(3)$ -invariant and $\mathbf{v}^{(k)} = \frac{\partial z^{(k)}}{\partial \mathbf{f}^{(k)}}$ remain $\text{SO}(3)$ -equivariant.

The outputted $\text{SO}(3)$ -equivariant features, i.e., $\mathbf{o}^{(K)}$, as well as the outputted $\text{SO}(3)$ -invariant features, i.e., $\mathbf{z}^{(K)}$, from the final (K th) layer of the encoding modules, are fed into the corresponding decoding modules to yield the predictions of \mathbf{Q} and $\mathbf{T} = \text{tr}(\mathbf{Q} \cdot \mathbf{Q}^\dagger)$, respectively. Since complex non-linear transformations have already been incorporated in the encoding framework, the decoders can be simple: the $\text{SO}(3)$ -equivariant decoder is implemented using an $\text{SO}(3)$ -equivariant linear mapping [20], and the $\text{SO}(3)$ -invariant decoder is implemented as a shallow feed-forward module.

8.2 Training and Inference

The training loss function is shown as the following:

$$\begin{aligned} \min_{\theta} \text{loss} &= \text{loss}_Q + \mu(\text{loss}_Q, \text{loss}_T) \cdot \text{loss}_T, \\ \text{loss}_Q &= \text{MSE}(\widehat{\mathbf{Q}}, \mathbf{Q}^*), \\ \text{loss}_T &= \text{MSE}(\widehat{\mathbf{T}}, \mathbf{T}^*) \end{aligned} \tag{10}$$

where θ denote all of the learnable parameters of our framework, $\widehat{\mathbf{Q}}$, $\widehat{\mathbf{T}}$ and \mathbf{Q}^* , \mathbf{T}^* respectively denote the predictions and labels of \mathbf{Q} and \mathbf{T} . In order that the both of the $\text{SO}(3)$ -equivariant and $\text{SO}(3)$ -invariant branches can be stably converged, we introduce $\mu(\text{loss}_Q, \text{loss}_T)$, i.e., a function returning a coefficient to regularize the relative scale of the two loss terms:

$$\mu(\text{loss}_Q, \text{loss}_T) = \lambda \cdot \text{No_Grad}\left(\frac{\text{loss}_Q}{\text{loss}_T}\right) \tag{11}$$

where $\text{No_Grad}(\cdot)$ denotes gradient discarding when calculating such coefficient, as this coefficient is only used for adjusting the relative scale of the two loss terms and should not itself be a source of training gradients, otherwise it would counteract loss_T in Equation (10). λ here is a hyperparameter, whose value is determined as 0.3 based on the performance on the validation set. The introduction of $\mu(\text{loss}_Q, \text{loss}_T)$ effectively prevents the numerical disparity between the two loss terms to stabilize the training for both of them.

In our framework, the $\text{SO}(3)$ -invariant non-linear features $z^{(k)} (1 \leq k \leq K)$ learned with the help of \mathbf{T} contribute to the learning of $\text{SO}(3)$ -equivariant representations $\mathbf{v}^{(k)} (1 \leq k \leq K)$ and the prediction of \mathbf{Q} . To achieve this goal, in the training phase, both the $\text{SO}(3)$ -invariant feature encoder and the $\text{SO}(3)$ -invariant decoder, used for predicting \mathbf{T} from $z^{(k)}$, need to be trained. While in the inference phase, since \mathbf{T} is not the final regression target, the $\text{SO}(3)$ -invariant decoder can be removed, yet the $\text{SO}(3)$ -invariant encoder still should be retained, used to induce $\text{SO}(3)$ -equivariant features.

9 Acknowledgements

This work was supported by the National Natural Science Foundation of China (Grant Number 12134012) and the Strategic Priority Research Program of Chinese Academy of Sciences (Grant Number XDB0500201).

References

- [1] Zhang, X., Wang, L., Helwig, J., Luo, Y., Fu, C., Xie, Y., Liu, M., Lin, Y., Xu, Z., Yan, K., Adams, K., Weiler, M., Li, X., Fu, T., Wang, Y., Yu, H., Xie, Y., Fu, X., Strasser, A., Xu, S., Liu, Y., Du, Y., Saxton, A., Ling, H., Lawrence, H., Stärk, H., Gui, S., Edwards, C., Gao, N., Ladera, A., Wu, T., Hofgard, E.F., Tehrani, A.M., Wang, R., Daigavane, A., Bohde, M., Kurtin, J., Huang, Q., Phung, T., Xu, M., Joshi, C.K., Mathis, S.V., Azizzadenesheli, K., Fang, A., Aspuru-Guzik, A., Bekkers, E., Bronstein, M., Zitnik, M., Anandkumar, A., Ermon, S., Liò, P., Yu, R., Günnemann, S., Leskovec, J., Ji, H., Sun, J., Barzilay, R., Jaakkola, T., Coley, C.W., Qian, X., Qian, X., Smidt, T., Ji, S.: Artificial intelligence for science in quantum, atomistic, and continuum systems. arXiv preprint arXiv:2307.08423 (2023)
- [2] Hohenberg, P., Kohn, W.: Inhomogeneous electron gas. *Physical Review* **136**(3B), 864 (1964)
- [3] Kohn, W., Sham, L.J.: Self-consistent equations including exchange and correlation effects. *Physical Review* **140**(4A), 1133 (1965)
- [4] Unke, O., Bogojeski, M., Gastegger, M., Geiger, M., Smidt, T., Müller, K.-R.: Se(3)-equivariant prediction of molecular wavefunctions and electronic densities, vol. 34, pp. 14434–14447 (2021)
- [5] Gu, Q., Zhang, L., Feng, J.: Neural network representation of electronic structure from ab initio molecular dynamics. *Science Bulletin* **67**(1), 29–37 (2022)
- [6] Li, H., Wang, Z., Zou, N., Ye, M., Xu, R., Gong, X., Duan, W., Xu, Y.: Deep-learning density functional theory hamiltonian for efficient ab initio electronic-structure calculation. *Nature Computational Science* **2**(6), 367–377 (2022)
- [7] Gong, X., Li, H., Zou, N., Xu, R., Duan, W., Xu, Y.: General framework for e (3)-equivariant neural network representation of density functional theory hamiltonian. *Nature Communications* **14**(1), 2848 (2023)
- [8] Guo, Y., Wang, H., Hu, Q., Liu, H., Liu, L., Bennamoun, M.: Deep learning for 3d point clouds: A survey. *IEEE Transactions on Pattern Analysis and Machine Intelligence* **43**(12), 4338–4364 (2020)
- [9] Qian, R., Lai, X., Li, X.: 3d object detection for autonomous driving: A survey. *Pattern Recognition* **130**, 108796 (2022)

- [10] Liao, Y., Smidt, T.E.: Equiformer: Equivariant graph attention transformer for 3d atomistic graphs. In: International Conference on Learning Representations (2023)
- [11] Musaelian, A., Batzner, S., Johansson, A., Sun, L., Owen, C.J., Kornbluth, M., Kozinsky, B.: Learning local equivariant representations for large-scale atomistic dynamics. *Nature Communications* **14**(1) (2023)
- [12] Zhong, Y., Yu, H., Su, M., Gong, X., Xiang, H.: Transferable equivariant graph neural networks for the hamiltonians of molecules and solids. *npj Computational Materials* **9**(1), 182 (2023)
- [13] Zitnick, L., Das, A., Kolluru, A., Lan, J., Shuaibi, M., Sriram, A., Ulissi, Z.W., Wood, B.M.: Spherical channels for modeling atomic interactions. In: Conference on Neural Information Processing Systems (2022)
- [14] Passaro, S., Zitnick, C.L.: Reducing $SO(3)$ convolutions to $SO(2)$ for efficient equivariant gnns. In: International Conference on Machine Learning, pp. 27420–27438 (2023)
- [15] Liao, Y., Wood, B.M., Das, A., Smidt, T.E.: Equiformerv2: Improved equivariant transformer for scaling to higher-degree representations. In: International Conference on Learning Representations (2024)
- [16] Yin, S., Zhu, X., Gao, T., Zhang, H., Wu, F., He, L.: Harmonizing $so(3)$ -equivariance with neural expressiveness: a deep learning framework oriented to the prediction of electronic structure hamiltonian. arXiv preprint arXiv:2401.00744 (2024)
- [17] Resnick, R.: Introduction to Special Relativity, (1991)
- [18] Wang, Y., Mao, Q., Zhu, H., Deng, J., Zhang, Y., Ji, J., Li, H., Zhang, Y.: Multi-modal 3d object detection in autonomous driving: a survey. *International Journal of Computer Vision* **131**(8), 2122–2152 (2023)
- [19] Thomas, N., Smidt, T., Kearnes, S., Yang, L., Li, L., Kohlhoff, K., Riley, P.: Tensor field networks: Rotation-and translation-equivariant neural networks for 3d point clouds. arXiv preprint arXiv:1802.08219 (2018)
- [20] Geiger, M., Smidt, T.E.: e3nn: Euclidean neural networks. *CoRR abs/2207.09453* (2022)
- [21] Fuchs, F., Worrall, D.E., Fischer, V., Welling, M.: Se(3)-transformers: 3d roto-translation equivariant attention networks. In: Conference on Neural Information Processing Systems (2020)

- [22] Schütt, K.T., Gastegger, M., Tkatchenko, A., Müller, K.-R., Maurer, R.J.: Unifying machine learning and quantum chemistry with a deep neural network for molecular wavefunctions. *Nature Communications* **10**(1), 5024 (2019)
- [23] Wang, Y., Li, H., Tang, Z., Tao, H., Wang, Y., Yuan, Z., Chen, Z., Duan, W., Xu, Y.: DeepH-2: Enhancing deep-learning electronic structure via an equivariant local-coordinate transformer. *arXiv preprint arXiv:2401.17015* (2024)
- [24] Cao, Y., Fatemi, V., Fang, S., Watanabe, K., Taniguchi, T., Kaxiras, E., Jarillo-Herrero, P.: Unconventional superconductivity in magic-angle graphene superlattices. *Nature* **556**(7699), 43–50 (2018)
- [25] He, M., Cai, J., Zheng, H., Seewald, E., Taniguchi, T., Watanabe, K., Yan, J., Yankowitz, M., Pasupathy, A., Yao, W., et al.: Dynamically tunable moiré exciton rydberg states in a monolayer semiconductor on twisted bilayer graphene. *Nature Materials* (2024)
- [26] Schrodinger, E.: Quantisierung als eigenwertproblem. *Annalen der Physik* **384**(4), 361–376 (1926)
- [27] He, K., Zhang, X., Ren, S., Sun, J.: Deep residual learning for image recognition. In: *IEEE/CVF Computer Vision and Pattern Recognition Conference*, pp. 770–778 (2016)